Crystal fractionation by crystal-driven convection

Cansu Culha[1], Jenny Suckale[1], Tobias Keller[1,2], Zhipeng Qin[1]

[1]Stanford University, Department of Geophysics, 397 Panama Mall, Stanford CA 94305, USA.
[2]University of Glasgow, School of Earth and Geographical Sciences, 8NN University Avenue, Glasgow G12 8QQ, UK.

Key Points:

- Crystals in liquid-rich environments settle efficiently and fractionate as crystal-rich clusters.
- Collective settling increases the efficiency of fractional crystallization compared to individual settling but depends on crystallinity.
- Depending on cluster dynamics, adjacent crystals may have been exposed to different melt environments leading to different zoning patterns.

Corresponding author: Cansu Culha, `cculha@stanford.edu`

Abstract

Fractional crystallization is an essential process proposed to explain worldwide compositional abundances of igneous rocks. It requires crystals to precipitate from the melt and segregate from its residual melt, or crystal fractionation. The compositional abundances of volcanic systems show a bell-curve distribution suggesting that the process has variable efficiencies. We test crystal fractionation efficiency in convective flow in low to intermediate crystallinity regime. We simulate the physical segregation of crystals from their residual melt at the scale of individual crystals, using a direct numerical method. We find that at low particle Reynolds numbers, crystals sink in clusters. The relatively rapid motion of clusters strips away residual melt. Our results show cluster settling can imprint observational signatures at the crystalline scale. The collective crystal behavior results in a crystal convection that governs the efficiency of crystal fractionation, providing a possible explanation for the bell curve distribution in volcanic systems.

1 Introduction

The worldwide compositional abundances of igneous rocks, including both volcanic and plutonic settings, show bimodal peaks at basaltic and rhyolitic compositions, referred to as the Daly gap (Daly, 1925). One of the key processes contributing to the formation of compositional gaps is fractional crystallization (Clague, 1978; Dufek & Bachmann, 2010; Jackson et al., 2018), a reactive transport process that requires crystals to precipitate from the melt and segregate from their residual melt. While some authors (e.g., Bonnefoi et al., 1995) have hypothesized that fractional crystallization leads to even distributions of composition, studies of compaction show variable efficiency of fractional crystallization (Dufek & Bachmann, 2010; Jackson et al., 2018).

A closer look at the worldwide compositional abundances reveals that their distribution is different in volcanic as compared to plutonic systems. Volcanic systems exhibit a single peak at basaltic compositions, whereas plutonic systems are characterized by a bimodal distribution with peaks at both basaltic and rhyolitic compositions (e.g. Chayes, 1963; Reubi & Blundy, 2009; Lee & Bachmann, 2014; Keller et al., 2015). The fundamental difference in the compositional distributions for the two settings suggests a corresponding difference in the processes governing magma evolution with compaction-driven fractional crystallization being more relevant in the plutonic rather than the volcanic setting.

The goal of this letter is to quantify the variable efficiency of fractional crystallization at low to intermediate crystal fraction. Our study is motivated by understanding the distribution of compositions in volcanic settings, which tend to be characterized by melts with less than 50% crystallinity prior to an eruption (Vigneresse et al., 1996; Jicha et al., 2005; Wieser et al., 2019a). We focus specifically on the segregation component of fractional crystallization, which we refer to as crystal fractionation (e.g., Bowen, 1928). We hypothesize that crystal-crystal interactions increase the efficiency of fractional crystallization by triggering a transition from individual to collective settling.

We test our hypothesis through direct numerical simulations that resolve the crystal-melt interactions at the scale of individual crystals (Suckale et al., 2012a; Qin & Suckale, 2017). As a consequence, we do not require any *a priori* parametrizations of phase-interactions such as effective viscosity, segregation drag, or settling speed. Instead, these quantities emerge self-consistently from simulations. Our simulations hence allow us to quantify the nonlinear ramifications of complex physical processes, such as the dynamic, long-range interaction between crystals, at the scale of individual crystals. An attractive attribute of our model approach is that it is testable against crystalline-scale data and could enable an assessment of the processes leading to fractional crystallization at the field-site

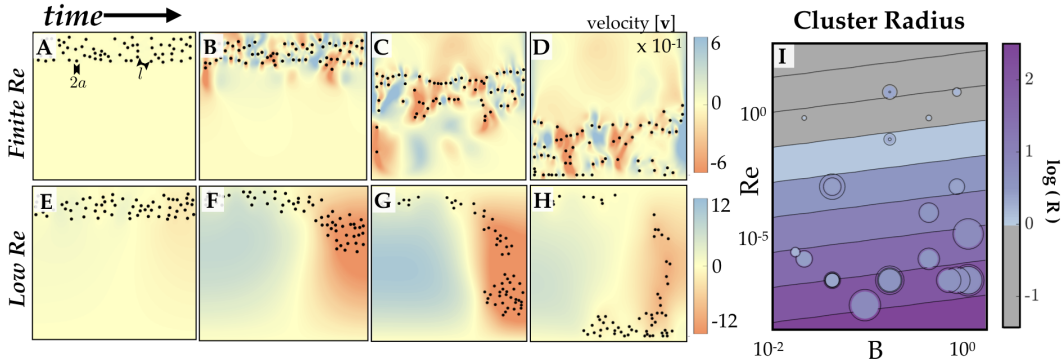

Figure 1. Varying degree of collectivity in crystal settling. Temporal snapshots from two different simulations at finite (A–D) and low (E–H) particle Reynolds number (Re). Both simulations have the same B value. They both show a form of collective motion between the crystals, but the degree of collectivity is more pronounced at low Re. (I) summarizes the degree of collectivity as estimated by the size of the crystal-rich cluster for different Re and B. In (I), the size of the circles indicate the size of the cluster relative to crystal radius. Each circle in the diagram is a simulation. The magnitude size of the clusters, R_m and the background colors, R indicate crystal cluster size relative to crystal radius as described by Supp. Sec. 2.

scale. To demonstrate the potential of the model in this regard, we compare our simulation results to variability observed in compositional profiles of plagioclase crystals in a fractionating basalt from Philpotts et al. (1998).

Our study builds the necessary theoretical foundation for intuition derived from observational studies (Wadsworth, 1973; Mathews et al., 1964; Moore & Evans, 1967) that crystal settling appears to occur either through a single descending column of crystal-rich liquid (Hess, 1960; Irvine, 1980) or "tear-drop-like masses"(Hess, 1960). Similarly, Sparks et al. (1984) suggested that crystal fractionation occurs in a "wide variety of convective phenomena caused by crystallization" such as in crystal-rich downwellings. By isolating the segregation effects of crystal-melt interactions, we are able to focus our contribution on identifying the physical processes leading to crystal-driven convective flow and to quantify the efficiency of melt-crystal segregation in this regime. By zooming into the crystalline scale process, we are also able to record the possible observational signatures of crystal-driven convection. We compare our results to crystalline data from Holyoke basalt flow, which is hypothesized to record fractional crystallization in crystal core to margin profiles (Philpotts et al., 1998).

2 Collective flow dominates in the Stokes limit.

To understand crystal fractionation in crystal-driven convection, we employ an idealized model set up where the upper boundary layer represents a cooling interface with negatively buoyant crystals suspended above a crystal-free melt body. We assume that the melt phase has constant density and viscosity, which means that the ensuing flow is entirely driven by the crystal-melt buoyancy contrast. Therefore, we are able to isolate crystal fractionation due to crystal-driven convection apart from other potentially confounding factors.

A key control on the degree of collective flow during crystal settling is the relative importance of inertial and viscous forces. This relationship is represented in the non-dimensional

Reynolds number, $\mathrm{Re} = a\Delta u\rho_\ell/\mu_\ell$, where Δu is the characteristic crystal-melt segregation speed which we take as the Stokes settling speed of a single crystal; a, g ρ_ℓ, and μ_ℓ are crystal radius, gravity, melt density, and dynamic melt viscosity, respectively. Another important contribution to collective flow is crystal distribution, which we describe by the non-dimensional number $\mathrm{B} = \phi a/l$. The number B combines the complementary scales of the crystal radius, the characteristic crystal spacing, l, and the crystal volume fraction or crystallinity, ϕ (Faroughi & Huber, 2015; Shibano et al., 2012). It expresses how varying the crystal spacing, l, at a given crystallinity, ϕ, will distinguish the contrasting scenarios of either a few large or many more small crystals.

For our analysis, we use a dimensional solver (Qin & Suckale, 2017; Qin et al., 2019), but to facilitate a comparison to other contexts, we non-dimensionalize our equations and results using the parameters provided above. We provide details on the methods and set up in Supp. Sec. 1. More details on the numerical method and benchmarks are available in Suckale et al. (2012b); Qin & Suckale (2017) and Qin et al. (2019).

In Figure 1A–H, we compare two simulations with different liquid viscosity but identical parameters in the solid phase. The higher viscosity could represent crustal-scale melt bodies, while the lower viscosity could be applicable to magma oceans.

Figure 1 shows two simulations at different Re with B held constant. We observe a higher degree of collective flow in the viscously-dominated ($\mathrm{Re}< 1$) compared to the inertially-dominated ($\mathrm{Re}\geq 1$) regime, which is apparent both from the evolving distribution of crystals, as well as from the vertical melt speed. In the inertial regime (panels A–D), crystals begin settling individually, but over time arrange into settling trains forming as a consequence of low-pressure wakes. In the viscous regime (panels E–H), crystals and melt organize into a broad cluster of crystals and melt settling collectively.

To quantify under what conditions collective flow dominates over individual settling, we compute the mean wavelength of the horizontal distribution of vertical speed, the measured cluster radius, R_m, for a range of Re and B values (see Supp. Sec. 2 for measuring R_m). In Fig. 1I, we show how the measured cluster radius varies with Re and B. We observe a continuous transition from individual crystals or crystal clusters consisting of two or three crystals to the formation of mesoscale clusters that include tens of crystals with increasing Re and B (Fig. 1).

To verify the robustness of our results, we run multiple simulations with randomly placed crystals to obtain a range of initial conditions. We find that the stochasticity and the non-linearity of crystal-melt interactions results in some variation in R_m even at identical Re and B. Nevertheless we find an overall consistent trend, with R_m comparable in size to the crystal radius at finite Re and low B, and R_m on the scale of the domain dimensions at low Re and high B.

We derive a characteristic scale for the cluster radius, R, by taking the ratio of the characteristic rates of viscous diffusion and inertial advection of momentum in Supp. Sec. 2. We show this relation as Fig. 1I background color. The observed trend of increasing cluster size, and hence increasing degree of flow coordination, in our simulations is consistent with our dimensional analysis.

3 Crystal rich clusters lead to efficient fractionation

After characterizing collective settling, we test whether crystals fractionate more or less efficiently in collective compared to individual settling. To quantify the degree of crystal fractionation, we run multiple simulations at the same low Re but variable B numbers.

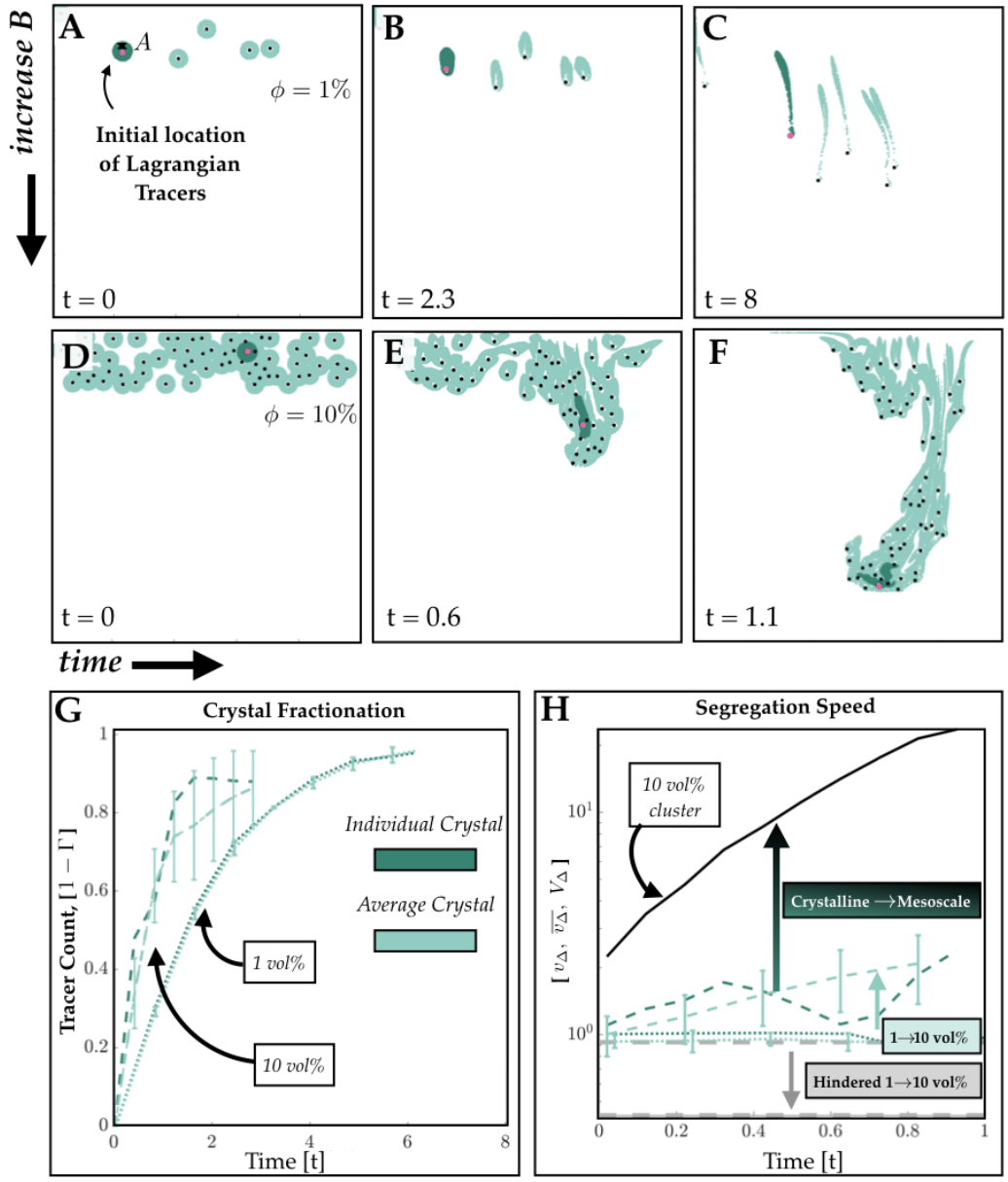

Figure 2. Characterizing crystal fractionation in individual and collective settling. We show two simulations at the same Re of 4×10^{-6} and different B values of 0.004 (A–C) and 0.4 (D–F). Simulation of crystals segregating from the residual melt (turquoise tracers) at 1 vol% (A–C) and 10 vol% (D–F) crystallinity. We pick a crystal in red and its residual tracers in dark turquoise to track over time. (G) Number of residual tracers in the control volume around the crystals, Γ, to quantify the degree of fractionation, $(1-\Gamma)$, for the two simulations. The dark turquoise curve highlights the degree of fractionation for the red crystals in (A-F) as a comparison point for the average behavior (light turquoise). (H) Comparison of the segregation speeds. The black line is the cluster speed, identified as the mesoscale segregation speed, V_Δ, from the melt around the cluster. The two gray lines show the hindered-settling speeds at 1 vol% (top line) and 10 vol% (bottom line) crystallinity.

We introduce Lagrangian tracers to track the melt initially surrounding each crystal, which, depending on the element of interest, may be depleted or enriched during crystal growth (turquoise in Fig. 2) as opposed to the background melt unaffected by crystallization (white). We initialize the residual melt tracers in a circular area around the crystal to represent a diffusively depleted rim of radius $A = 3a$ around the crystal (see Supp. Mat. 3 for discussion on A). As crystals settle in the low crystallinity case (1 vol%), individual crystals uniformly strip away the residual melt. Whereas, at 10 vol% crystallinity, crystals fractionate less uniformly.

To quantify the degree of crystal fractionation, we count the number of residual melt tracers that originated around each crystal compared to the total number of tracers within the same control area of radius, A, at each time step. If the ratio of residual tracers to total number of tracers, Γ, in the control area is 1 then no crystal fractionation has occurred. If the ratio is 0, then the crystal is completely stripped of its residual melt, completing crystal fractionation. Therefore, $(1-\Gamma)$ indicates the degree of crystal fractionation for an individual crystal. The average degree of crystal fractionation is the average of this metric over all of the crystals.

Our results show that both individually settling crystals (Fig. 2A–C) and collectively settling crystals (Fig. 2D–F) fractionate from their residual melt. However, clusters generally do not fully reach the same degree of fractionation as individually settling crystals. For the two simulations shown in Fig. 2, the rate of average crystal fractionation, represented by the slopes of curves in Fig. 2 G, is a factor of two faster at 10 vol% as compared to 1 vol% crystallinity. While the precise factor of speedup varies, our full ensemble of simulations with varying A, domain size and initial crystal placement show robustly that the rate of crystal fractionation is comparable to or faster than individual crystal fraction (Supp. Sec. 4).

Next, we quantify the segregation speeds that ultimately control the rate of crystal fractionation in Fig. 2H. We define the individual crystal-melt segregation speed as $v_\Delta = |\mathbf{v_\Delta}| = |\mathbf{v_c} - \overline{\mathbf{v}_\ell}|$, where $\mathbf{v_c}$ and $\mathbf{v}_\ell$ are the crystal and melt velocities. We measure the velocity difference between the crystal's center of mass and the average melt velocity within the control area of radius A. In Fig. 2H, the average metric shows a gradual increase in crystal-melt segregation speed with time for 10 vol% crystallinity, whereas the 1 vol% case reaches terminal velocity within a few time steps.

The finding that increasing crystallinity results in faster settling contrasts with the hindered-settling parametrization of average segregation speed. Derived from experiments and theory, hindered-settling implies slower settling speeds at higher crystallinities (e.g., Huppert et al., 1991; Arai & Maruyama, 2017). The crystals within the cluster experience hindered-settling relative to the melt in the cluster, but melt advection outside of the cluster rim increases the segregation speed of crystals along the rim. The average crystal segregation speed is thus greater than suggested by either hindered- or unhindered-settling parametrizations.

4 Crystal scale zoning signatures of convective fractionation

While fractional crystallization is difficult to observe directly in magmatic systems, our models suggest that collective settling imprints subtle, observational clues on crystal clusters (e.g., Wieser et al., 2019b; Schwindinger & Anderson, Jr., 1989) or crystal chains (Philpotts et al., 1998). We observe that each crystal in a collectively settling cluster segregates and thus fractionates at a slightly different rate depending on its location between the cluster center and rim. We first characterize this heterogeneity in individual crystal evolution in dark green lines of Fig. 2 and in more detail in Supp. Sec. 6. We hypothesize that this heterogeneity could be captured in crystalline cross-sectional pro-

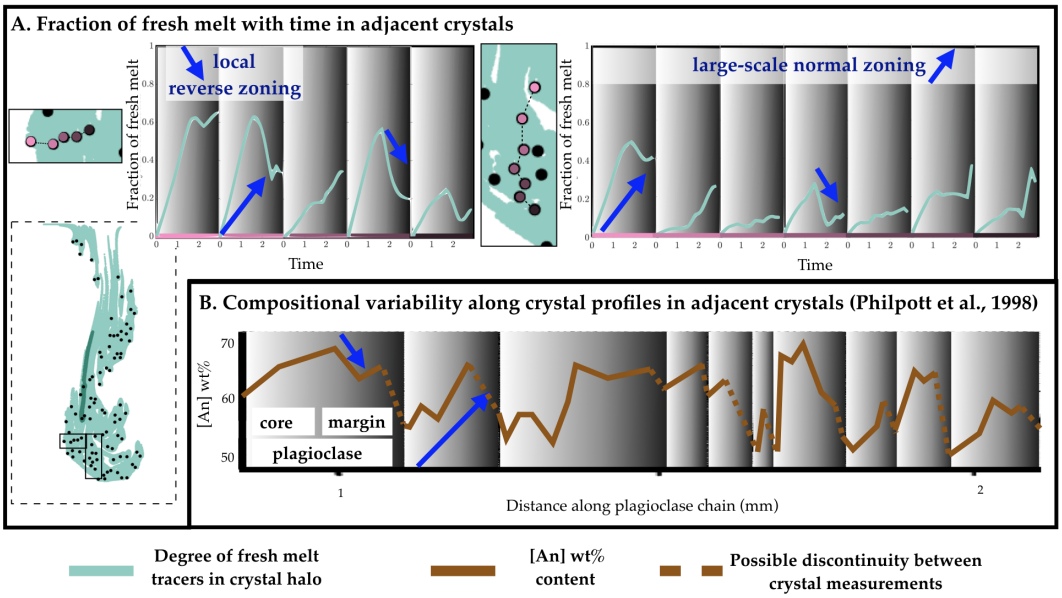

Figure 3. Crystalline scale variability with time and along crystal profile. In (A), we track the number of fresh melt tracers relative to initial number of tracers around each crystal halo through time. Time is from the start of the simulation to the moment of the simulation snapshot shown in the left. We zoom into 2 sets of adjacent crystals, which are identified from light pink to dark pink. We identify a large-scale normal zoning and a small-scale reverse zoning, which are indicated by the blue up and down arrows, respectively. In (B), we zoom into the anorthite content of 10 crystals by Philpotts et al. (1998).

files as crystal zonations, which have been associated with many processes (Wallace & Bergantz, 2005; Longpré et al., 2014; Wolff et al., 2015).

To demonstrate the testability of our model against crystalline-scale data, we compare our results to the 174-m-thick Holyoke basalt flow, which is thought to have experienced fractional crystallization post eruption (Philpotts & Carroll, 1996) with continuous transport of plagioclase crystals from roof to bottom of the flow (Philpotts & Dickson, 2000) at intermediate crystallinity (< 50 vol%; Philpotts et al., 1998). We use the plagioclase crystals in the melt that formed during fractional crystallization (Philpotts et al., 1998) as markers sampling the process.

To quantify the melts that a crystal would sample in our simulations, we track the different types of melt in the system, namely: fresh melt versus evolved melt. We use a complementary description to the analysis in Fig. 2G. Here, all residual melt tracers are identified as evolved melt tracers, $\tilde{\Gamma}$. In Fig. 3A, we plot the fraction of fresh melt tracers, $(1-\tilde{\Gamma})$, present in the crystal halo for adjacent crystals from the start until the time displayed in the snapshot in Fig. 3A.

We look at the fraction of fresh melt exposure around crystals as it changes with time. A single trajectory of a simulation crystal (first profile in Fig. 3A) shows the crystal losing some of the residual melt and entering into an environment with more fresh melt. Once it reaches about 60 % fresh melt, it gets exposed to more residual melt again before once more entering into an environment with more fresh melt. We observe that (1) on a larger time scale, each crystal gets exposed to greater amounts of fresh melt tracers with time, which would imprint as large-scale normal zoning and (2) on a smaller time scale, each crystal may experience a relative decrease in fresh melt exposure with time,

which would likely imprint as small-scale reverse zoning. Additionally, neighboring crystals may experience different melt histories during collective settling.

Depending on crystal growth rates, crystals may grow or dissolve rims representing the composition of the melt surrounding the crystals (Ruprecht et al., 2008). Crystal growth rates can be as fast as 10^{-6} mm/s (Couch, 2003). At this rate, the small time scale reverse zoning (roughly lasting for 1 dimensionless unit of time) would be preserved in crystalline structure as $10^{-4} - 1$ mm rim for viscosity values of 10^{2-6} Pa·s.

Our results suggest that each crystal may record different sequences of melt environments as it settles though the magma layer with time. We compare the exposure to different melt compositions in our simulation to anorthite content variations in the Holyoke basalt flow plagioclase crystals, where the behavior of large scale normal zoning and small scale reverse zoning in adjacent crystals has been measured (Philpotts et al., 1998). Fig. 3B shows the cross sectional anorthite content of adjacent plagioclase crystals as first shown in Philpotts et al. (1998). The original plot includes 14 crystals with different sizes, obscuring the patterns from crystal core (white) to margin (black). Therefore, we increase the size of 10 crystal profiles to increase visibility of the profiles. Additionally, Philpotts et al. (1998) has the crystal margin connected to the core of the adjacent crystal (brown dashed lines). Since the anorthite content from one crystal margin to another crystal core should be discontinuous, we connect the compositional profiles with brown dashed lines at the last identifiable measurement.

These crystals consistently show a large-scale increase in anorthite content with small zones of decreasing anorthite content. Based on anorthite phase diagrams, batch crystallization could not explain the increase in anorthite content as magma cools. Therefore, increase in anorthite content suggests that the crystals are getting exposed to more mafic magma. The anorthite content is hence analogous to "fresh magma" in our simulations. Although we provide a very simple model where we do not track anorthite content or model the growth of crystals, tracking of residual and fresh melt tracers allows us to capture how crystals can inherit zoning patterns that are comparable to anorthite content patters captured in Philpotts et al. (1998) by migrating through different domains in a collectively settling clusters and thereby getting exposed to different melt compositions.

5 Efficiency depends on crystallinity and crystal distribution

Reactive processes are essential for describing compositional alterations, but they alone do not explain the change in bulk compositions without crystal fractionation. Therefore, the efficiency of crystal fractionation is significant for quantifying efficiency of fractional crystallization. The efficiency at which crystals collectively strip away from their residual melt is a function of many parameters, but to the first order, it is a function of cluster speed. Additionally, as the cluster sinks, the boundary where crystals initially formed will be replaced by the return flow of the hotter, less evolved magma. As the fresh magma becomes exposed to the cooling boundary layer it will form and grow more crystals, resulting in a self-sustaining convection cell. We use cluster-melt segregation speed as the critical speed to describe the efficiency of collective fractionation.

For the simulations that show collective motion, we measure how fast crystals force magma overturn by measuring the cluster-melt segregation speed, $V_\Delta = |\mathbf{V_\Delta}| = |\mathbf{v_d} - \overline{\mathbf{v}_\ell}|$, where $\mathbf{v_d}$ is the cluster velocity, the mean velocity of the crystals within the cluster area and $\overline{\mathbf{v}_\ell}$ is the average melt velocity within $2R_m$ away from cluster center of mass. We approximate the cluster center of mass as the center of mass of the crystals and define the cluster bounds by R_m.

Our analysis suggests that, in the highly simplified case in Fig. 2, a crystal cluster can advect 100 m through melt viscosity of 10^2 Pa·s in 12 days. In contrast, individ-

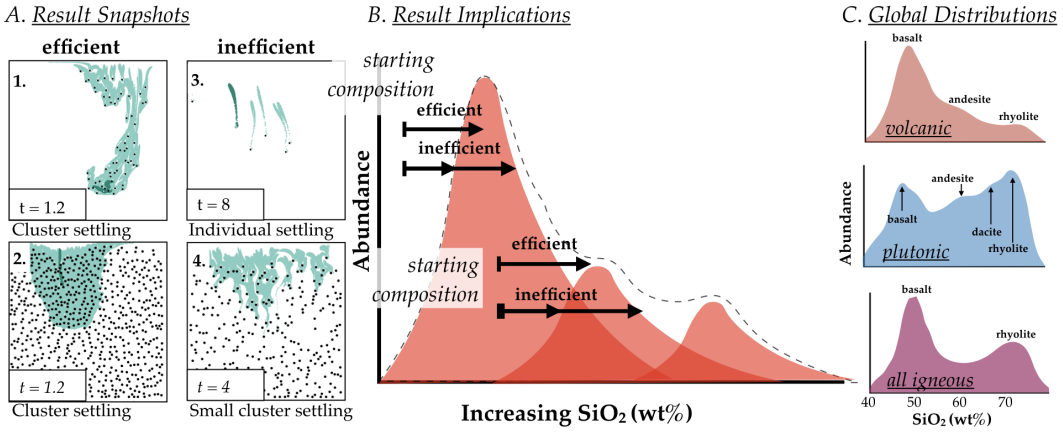

Figure 4. Constant low Re with variable crystallinity and crystal distribution. We show 4 simulation snapshots in (A). We show snapshots with crystallinity difference between top and bottom layers. Simulation (1–3) have 10 over 0, 30 over 20, and 1 over 0 vol% crystallinity, respectively. Sim (4) has 10 vol% crystallinity everywhere. We quantify the efficiency of crystal fractionation in Supp. Sec. 5. In (B), we illustrate the efficiency implications of our results on the compositional abundances as bell curves. The peak composition of the first bell curve would be the new starting composition for further fractional crystallization, forming a new bell curve. Adding these abundance curves could produce the dotted black line. Figure C shows the global distributions of volcanic, plutonic, and all igneous systems as a function of SiO_2 content in arc settings as originally presented in Keller et al. (2015).

ual settling at low crystallinity would cover the same distance in 331 days, resulting in negligible magma overturn, and hence less efficient compositional segregation and fractional crystallization.

We suggest that a hot magma injected into a magma processing zone would initially begin to cool at the boundaries, creating a sharp gradient in crystallinity and efficiently advecting crystal clusters. Our results summarized in Fig. 4A show this efficiency varies depending on crystallinity and crystal distribution. If the magmatic lens reaches equilibrium with its surrounding melt, it will form crystals everywhere (Fig. 44A) or lose most of its crystals to cluster settling (Fig. 43A). It is also possible that the lens has high crystallinity everywhere. Compaction (e.g., Richter & McKenzie, 1984), the crystal fractionation model that best describes high crystallinity regime, would compress melt with viscosity of 10^2 Pa·s 100 m in 600 years, which is orders of magnitude slower than cluster fractionation.

There are many factors that contribute to efficient and inefficient modes of fractional crystallization. In Fig. 4B, we illustrate that the different modes would result in a bell curved bulk composition distribution in large scale data sets. In the figure, we do not provide bulk silica content values on the x-axis because both petrology and crystal fractionation would define the location and distribution of the peak.

We suggest that magmatic lenses from the mantle would fractionate resulting in the first distribution. Volcanic eruptions would sample the initial distribution or stay trapped as new magmatic lenses in disequilibrium. The new lenses would be the starting composition for further fractionation, forming a new bell curve distribution. In the figure, we show each of the bell curves decreasing in abundance with increase in silica content, to tell a simple story that the daughter distributions will be smaller than mother

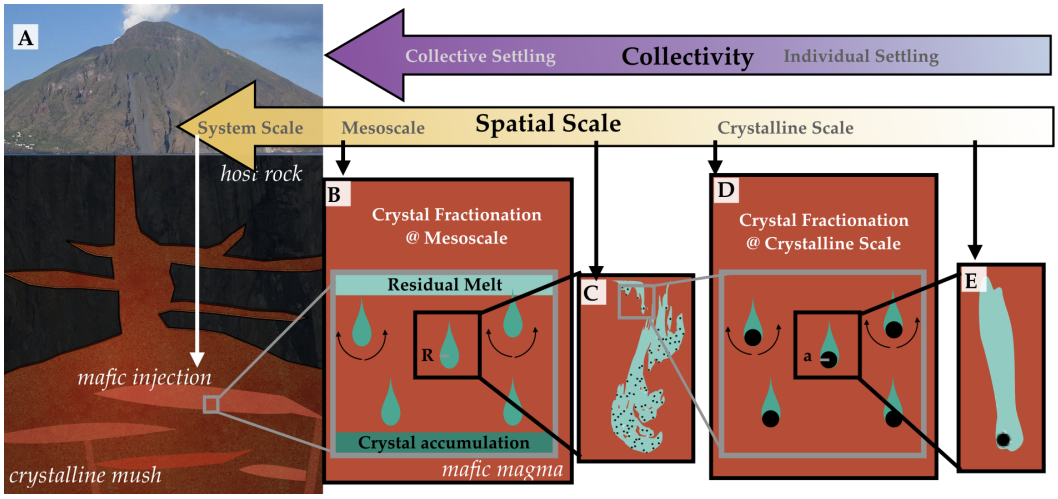

Figure 5. Summary of scales: Zooming into the mafic injection (A), we argue that crystal settling can be conceptualized through mesoscale clusters (B) that lead to efficient but heterogeneous fractionation as demonstrated by our numerical results (C). Further zooming into the cluster would show that melt is stripped from each crystal individually as plotted schematically in (D) and demonstrated in our numerical result in (E) and Fig. 2E-H).

distributions; however, this might not be true if certain areas preferentially have an easier time fractionating then erupting instead of erupting the original distribution. Combining these bell curve histograms would add up to a distribution that resembles the compositional distribution of volcanic systems shown in Fig. 4C. However it does not resemble the plutonic distribution. Plutonic outcrops show vast regions that experienced alteration for millions of years at high crystallinity prior to exposure (Coleman et al., 2004; Deering et al., 2016). The collective settling processes discussed here are hence more pertinent for the volcanic rather than the plutonic context.

6 Conclusions

Large scale convective drivers set the reference frame at which we study crystal cluster settling in trans-crustal mush bodies. Despite differences in dynamics, there is a striking self-similarity between the crystalline-scale and the mesoscale settling. Like a single crystal settling, a cluster strips away the residual melt around itself. In Fig. 5, we provide a conceptual summary of crystal-driven convective fractionation at the mesoscale as understood based on our simulations. The key difference between the two scales is the increased speed at which mesoscale clusters sink through the magma compared to individual crystals. We only study the crystal fractionation component of fractional crystallization. We do not consider reactive processes like melt density differences, which may further enhance the efficiency of fractional crystallization. Outside of crystal resorption and bubble formation, it is reasonable to expect that our estimates for the efficiency of crystal fractionation by collective settling are a lower bound.

Acknowledgments

The authors would like to thank George Bergantz, Shan de Silva, Christy Till, Gail Mahood, Ayla Pamukcu and David Pollard for fruitful discussions throughout the development of the project. CC acknowledges support from the NSF's GRFP and Stanford University's McGee Grant. TK acknowledges support from the Swiss National Science

348 Foundation's Postdoc.Mobility Fellowship 177816. See Supplementary Material and our
349 GitLab repository: git@zapad.Stanford.EDU:cansu.culha/crystal-fractionation.git for codes.
350

References

Arai, T., & Maruyama, S. (2017). Geoscience Frontiers Formation of anorthosite on the Moon through magma ocean fractional crystallization. *Geosci. Front.*, *8*(2), 299–308. Retrieved from http://dx.doi.org/10.1016/j.gsf.2016.11.007 doi: 10.1016/j.gsf.2016.11.007

Bonnefoi, C. C., Provost, A., & Albarède, F. (1995). The Daly gap' as a magmatic catastrophe. *Nature*, *378*(6554), 270–272. doi: 10.1038/378270a0

Bowen, N. (1928). The evolution of the Igneous Rocks. *Dover Publ.*.

Chayes, F. (1963). Relative abundance of intermediate members of the oceanic basalt-trachyte associatio. *J. Geophys. Res.*, *68*(5), 1519–1534.

Clague, D. A. (1978). The Oceanic Basalt-Trachyte Association : An Explanation of the Daly Gap. *J. Geol.*, *86*(6), 739–743.

Coleman, D. S., Gray, W., & Glazner, A. F. (2004). Rethinking the emplacement and evolution of zoned plutons: Geochronologic evidence for incremental assembly of the Tuolumne Intrusive Suite, California. *Geology*, *32*(5), 433–436. doi: 10.1130/G20220.1

Couch, S. (2003). Experimental investigation of crystallization kinetics in a haplogranite system. *American Mineralogist*, *88*(10), 1471–1485.

Daly, R. A. (1925). The Geology of Ascension Island. *Proc. Am. Acad. Arts Sci.*, *60*(1), 3–80.

Deering, C. D., Keller, B., Schoene, B., Bachmann, O., Beane, R., & Ovtcharova, M. (2016). Zircon record of the plutonic-volcanic connection and protracted rhyolite melt evolution. *Geology*, *44*(4), 267–270. doi: 10.1130/G37539.1

Dufek, J., & Bachmann, O. (2010). Quantum magmatism: Magmatic compositional gaps generated by melt-crystal dynamics. *Geology*, *38*(8), 687–690. Retrieved from http://geology.gsapubs.org/cgi/doi/10.1130/G30831.1 doi: 10.1130/G30831.1

Faroughi, S. A., & Huber, C. (2015). Unifying the relative hindered velocity in suspensions and emulsions of nondeformable particles. *Geophys. Res. Lett.*, *42*(1), 53–59. doi: 10.1002/2014GL062570

Hess, H. (1960). *Stillwater igneous complex, montana.* The Geologic Society of America Memoir 80.

Huppert, H. E., Kerr, R. C., Lister, J. R., & Turner, J. S. (1991). Convection and particle entrainment driven by differential sedimentation. *J. Fluid Mech.*, *226*, 349–369. doi: 10.1017/S0022112091002410

Irvine, T. (1980). Magmatic density currents and cumulus processes. *American Journal of Science*, *280*(Jackson Volume), 1–58.

Jackson, M. D., Blundy, J., & Sparks, R. S. (2018). Chemical differentiation, cold storage and remobilization of magma in the Earth's crust. *Nature*, *564*(7736), 405–409. Retrieved from http://dx.doi.org/10.1038/s41586-018-0746-2 doi: 10.1038/s41586-018-0746-2

Jicha, B. R., Singer, B. S., Beard, B. L., & Johnson, C. M. (2005). Contrasting timescales of crystallization and magma storage beneath the Aleutian Island arc. *Earth Planet. Sci. Lett.*, *236*(1-2), 195–210. doi: 10.1016/j.epsl.2005.05.002

Keller, C. B., Schoene, B., Barboni, M., Samperton, K., Husson, J. M., Hall, G., ... Angeles, L. (2015). Volcanic plutonic parity and the differentiation of the continental crust. *Nature*, *523*, 301—-307.

Lee, C. T. A., & Bachmann, O. (2014). How important is the role of crystal fractionation in making intermediate magmas? Insights from Zr and P systematics. *Earth Planet. Sci. Lett.*, *393*, 266–274. Retrieved from http://dx.doi.org/10.1016/j.epsl.2014.02.044 doi: 10.1016/j.epsl.2014.02.044

Longpré, M.-a., Klügel, A., Diehl, A., & Stix, J. (2014). Mixing in mantle magma reservoirs prior to and during the 2011 2012 eruption at El Hierro , Canary Is-

lands. *Geology*, 2012–2015. doi: 10.1130/G35165.1

Mathews, W., Thorarinsson, S., & Church, N. (1964). Gravitative settling of olivine in pillows of an icelandic basalt. *American Journal of Science*, *262*(8), 1036–1040.

Moore, J. G., & Evans, B. W. (1967). The role of olivine in the crystallization of the prehistoric makaopuhi tholeiitic lava lake, hawaii. *Contributions to Mineralogy and Petrology*, *15*(3), 202–223.

Philpotts, A. R., & Carroll, M. (1996). Physical properties of partly melted tholeiitic basalt. *Geology*, *24*(11), 1029–1032. doi: 10.1130/0091-7613(1996)024⟨1029:PPOPMT⟩2.3.CO;2

Philpotts, A. R., & Dickson, L. D. (2000). The formation of plagioclase chains during convective transfer in basaltic magma. *Nature*, *406*(6791), 59–61. doi: 10.1038/35017542

Philpotts, A. R., Shi, J., & Brustman, C. (1998). Role of plagioclase crystal chains in the differentiation of partly crystallized basaltic magma. *Nature*, *395*(September), 343–346.

Qin, Z., Alison, K., & Suckale, J. (2019). Rotation matters-direct numerical simulations of rectangular particles in suspensions at low to intermediate solid fraction. *arXiv preprint arXiv:1903.08167*.

Qin, Z., & Suckale, J. (2017). Direct numerical simulations of gassolidliquid interactions in dilute fluids. *Int. J. Multiph. Flow*, *96*(November), 34–47.

Reubi, O., & Blundy, J. (2009). A dearth of intermediate melts at subduction zone volcanoes and the petrogenesis of arc andesites. *Nature*, *461*(7268), 1269–1273. Retrieved from `http://dx.doi.org/10.1038/nature08510` doi: 10.1038/nature08510

Richter, F. M., & McKenzie, D. (1984). Dynamical models for melt segregation from a deformable matrix. *The Journal of Geology*, *92*(6), 729-740. Retrieved from `https://doi.org/10.1086/628908` doi: 10.1086/628908

Ruprecht, P., Bergantz, G. W., & Dufek, J. (2008). Modeling of gas-driven magmatic overturn: Tracking of phenocryst dispersal and gathering during magma mixing. *Geochemistry, Geophys. Geosystems*, *9*(7), 1–25. doi: 10.1029/2008GC002022

Schwindinger, K. R., & Anderson, Jr., A. T. (1989). Synneusis of Kilauea Iki olivines. *Contrib. Miner. Pet.*, *103*, 187—-198.

Shibano, Y., Namiki, A., & Sumita, I. (2012). Experiments on upward migration of a liquid-rich layer in a granular medium: Implications for a crystalline magma chamber. *Geochemistry, Geophys. Geosystems*, *13*(3). doi: 10.1029/2011GC003994

Sparks, R. S. J., Huppert, H. E., Turner, J. S., Sakuyama, M., & O'Hara, M. J. (1984). The Fluid Dynamics of Evolving Magma Chambers [and Discussion]. *Philos. Trans. R. Soc. A Math. Phys. Eng. Sci.*, *310*(1514), 511–534. Retrieved from `http://rsta.royalsocietypublishing.org/cgi/doi/10.1098/rsta.1984.0006` doi: 10.1098/rsta.1984.0006

Suckale, J., Elkins-Tanton, L. T., & Sethian, J. A. (2012b). Crystals stirred up: 2. numerical insights into the formation of the earliest crust on the moon. *Journal of Geophysical Research: Planets*, *117*(E8).

Suckale, J., Sethian, J., Yu, J., & Elkins-Tanton, L. (2012a). Crystals stirred up: 1. direct numerical simulations of crystal settling in nondilute magmatic suspensions. *Journal of Geophysical Research: Atmospheres*, *117*(8). doi: 10.1029/2012JE004066

Vigneresse, J. L., Barbey, P., & Cuney, M. (1996). Rheological transitions during partial melting and crystallization with application to felsic magma segregation and transfer. *J. Petrol.*, *37*(6), 1579–1600. doi: 10.1093/petrology/37.6.1579

Wadsworth, J. (1973). Magmatic sediments. *Mineral, Sci. Engng.*, *5*, 25–35.

Wallace, G. S., & Bergantz, G. W. (2005). Reconciling heterogeneity in crystal zoning data: An application of shared characteristic diagrams at Chaos Crags, Lassen Volcanic Center, California. *Contrib. to Mineral. Petrol.*. doi: 10.1007/s00410-004-0639-2

Wieser, P. E., Vukmanovic, Z., Kilian, R., Ringe, E., Holness, M. B., Maclennan, J., & Edmonds, M. (2019a). To sink, swim, twin, or nucleate: A critical appraisal of crystal aggregation processes. *Geology*, *47*(10), 948–952. doi: 10.1130/g46660.1

Wieser, P. E., Vukmanovic, Z., Kilian, R., Ringe, E., Holness, M. B., Maclennan, J., & Edmonds, M. (2019b). To sink, swim, twin, or nucleate: A critical appraisal of crystal aggregation processes. *Geology*, *47*(Xx), 1–5. Retrieved from `https://pubs.geoscienceworld.org/gsa/geology/article/573164/To-sink-swim-twin-or-nucleate-A-critical-appraisal` doi: 10.1130/G46660.1

Wolff, J. A., Ellis, B. S., Ramos, F. C., Starkel, W. A., Boroughs, S., Olin, P. H., & Bachmann, O. (2015). Remelting of cumulates as a process for producing chemical zoning in silicic tuffs: A comparison of cool, wet and hot, dry rhyolitic magma systems. *Lithos*, *236-237*, 275–286. Retrieved from `http://dx.doi.org/10.1016/j.lithos.2015.09.002` doi: 10.1016/j.lithos.2015.09.002